

Multiple-effect desiccant-based zero liquid discharge desalination systems

Sunil Pinnu, Sajjad Bigham*

Department of Mechanical Engineering-Engineering Mechanics, Michigan Technological University, 1400 Townsend Drive, Houghton, MI 49931-1295, USA

HIGHLIGHTS

- A novel multiple-effect desiccant-based ZLD system is proposed to improve energy efficiency of the ZLD desalination process.
- The new concept replaces energy-intensive MVC-based brine crystallizers with an energy-efficient thermally-driven counterpart.
- A comprehensive thermodynamic model was performed to evaluate performance of the system at different conditions.
- The proposed ZLD desalination system offers a 63% energy reduction compared with current ZLD systems.

ARTICLE INFO

Keywords:

Desalination
Zero liquid discharge
Sorption systems
Thermal vapor compression
Multiple effect distillation

ABSTRACT

State-of-the-art zero liquid discharge (ZLD) technologies are currently bound with either intensive use of high-grade electrical energy such as mechanical vapor compressors or high capital cost with environmental concerns such as evaporation ponds. The present study aims to address these issues by an innovative desiccant-based ZLD desalination system in which a multiple-effect distillation (MED) unit is uniquely embedded at the heart of an absorption-desorption system. Here, the MED and absorption systems are inherently coupled enabling both heat and mass transfer processes between a hypersaline brine slurry and a desiccant solution. The proposed technology employs an absorption-based thermally-driven vapor compressor concept to pressurize the vaporized brine of the ZLD crystallizer unit from a low-pressure absorber to a high-pressure desorber module. The low water vapor pressure environment required for the ZLD treatment is established by the strong hygroscopic properties of an aqueous lithium bromide (LiBr) salt capturing a large volume of water vapor from the brine slurry. This eliminates the need for energy-intensive electrically-driven mechanical vapor compressors currently employed in advanced brine crystallizers. Comprehensive thermodynamic modeling is performed to evaluate the energy efficiency and size of the system at different thermohydraulic conditions. The detailed analysis indicates that the thermal energy consumption of the proposed desiccant-based ZLD desalination system is 67 kWh of thermal energy per cubic meter of the distillate produced with a gained output ratio (GOR) of 10. This is 63% and 44% reductions in the ZLD energy consumption compared with advanced mechanical vapor compression and thermal evaporation based ZLD systems, respectively. Insights gained from the present study have a high potential to truly transform thermal desalination and, in particular, ZLD treatment industries.

1. Introduction

Freshwater scarcity due to population growth, pollution of water bodies, industrialization, and climate change has imposed a major threat to the prospect of the world economy, environmental sustainability, and human life quality. Desalination of sea, waste, or brackish water has been largely considered as a potential solution to growing concerns on freshwater demands [1]. Conventional desalination techniques, however, generate a substantial amount of a highly concentrated discharge brine significantly disturbing the aquatic environment, natural

hydrologic cycles, and public health quality. Zero liquid discharge (ZLD) systems, on the other hand, completely recover the liquid wastewater, thereby minimizing adverse environmental risks and high effluent disposal costs. Current ZLD systems are, however, inefficient to purify saline water with high total dissolved solids (TDS) concentration values ($TDS > 100,000$ ppm), and often unable to economically achieve ZLD operation desired in many industrial applications with high brine disposal costs [2].

In current ZLD systems, the saline brine is initially pH adjusted to minimize scaling potentials of heat exchanger surfaces utilized. The treated brine is then concentrated in a brine concentrator driven by a

* Corresponding author.

E-mail address: sbigham@mtu.edu (S. Bigham).

<https://doi.org/10.1016/j.desal.2021.114942>

Received 8 October 2020; Received in revised form 6 December 2020; Accepted 25 December 2020

Available online 16 January 2021

0011-9164/© 2021 Elsevier B.V. All rights reserved.

Nomenclature	
<i>Acronym</i>	
CAPEX	capital expenditure
DU	desorption unit
EDR	electro dialysis reversal
EES	engineering equation solver
FC	forced circulation
FD	freeze desalination
FO	forward osmosis
GOR	gained output ratio
HX	heat exchanger
LiBr	lithium bromide
LMTD	logarithmic mean temperature difference
MD	membrane distillation
MED	multiple effect desalination
MVC	mechanical vapor compressor
OPEX	operating expenditure
RO	reverse osmosis
RR	recovery ratio
SHX	solution heat exchanger
TDS	total dissolved solids
TTD	terminal temperature difference
ZLD	zero liquid discharge
<i>Greek letters</i>	
Φ	mass fraction
Δ	difference
ε	effectiveness of heat exchanger
<i>Symbols</i>	
A	surface area [m ²]
B	mass flowrate of brine [kg/s]
C	specific heat [kJ/kg-°C]
D	mass flowrate of distillate [kg/s]
F	mass flowrate of feed [kg/s]
h	enthalpy [kJ/kg]
m	mass flow rate [kg/s]
P	pressure [kPa]
Q	heat [kW]
T	temperature [°C]
U	heat transfer coefficient [kW/m ² -°C]
γ	specific volume [m ³ /kg]
\dot{w}	work done [kW]
X	salinity [g/kg]
x	solution concentration
<i>Subscripts</i>	
a	absorber
b	boiling
bd	blown down
c	condensing stream
cond	condenser
d	desorber
e	effect
f	flashing
fb	flash box
loop	circulation loop
n	last MED effect
p	constant pressure
sat	saturation point
shx	solution heat exchanger
sw	seawater
we	within the effect
<i>Superscripts</i>	
BC	brine crystallizer
in	inlet
out	outlet
prev	previous
FH	feed heater
FCHX	forced circulation Heat eXchanger

mechanical vapor compressor (MVC) enabling the thermal separation process to a salinity concentration of about 250,000 mg/L with a recovery ratio of 90–98% [3]. The typical energy consumption of an MVC-driven brine concentrator is about 20–39 kWh of high-grade electric energy per cubic meter of the distillate produced [3,4]. The concentrated brine rejected from the brine concentrator is then sent to a brine crystallizer for the salt crystallization process. Currently, state-of-the-art ZLD technologies are mainly limited to intensive usage of high-grade electrical energy through MVC-driven brine crystallizers with a typical energy consumption of 52–66 kWh electric energy per cubic meter of the water distilled [3]. An alternative crystallization approach is brine evaporation ponds offering lower operational costs. They are a more preferred method for sites with high evaporation rates and inexpensive lands [5]. Evaporation ponds, however, suffer from several major drawbacks including hazardous wastes contaminating the environment and large areas of land requirement [6,7]. Therefore, future ZLD systems need to be both energy-efficient and environmentally-friendly to address the shortcomings of current ZLD systems.

To improve the energy performance of a hypersaline ZLD treatment process, most existing desalination systems aim to minimize the volume of concentrated slurry entering the crystallizer unit. This is typically accomplished by maximizing the water recovery of the feedwater brine with a more energy-efficient desalination technique before the crystallization process. One such method is to integrate the reverse osmosis (RO) process with a brine crystallizer unit. The RO process is a pressure-driven, membrane separation technique with an excellent energy

efficiency of about 2 kWh of electric energy per cubic meter of the distillate produced [1]. The RO process, however, has an upper salinity level of about 70,000 ppm [8]. Therefore, many recent studies have examined the performance of a brine crystallizer integrated with other desalination technologies offering a higher upper salinity level than that of the RO process [9,10]; including membrane distillation (MD) [11,12], electrodialysis [13,14], forward osmosis (FO) [4], freeze desalination [15,16], and supercritical water [17].

To treat a RO discharge brine, a hybrid ZLD system using the electrodialysis reversal (EDR) and crystallization processes was studied by Oren et al. [13]. A super-concentrate brine with over 10% TDS from the EDR unit was further concentrated in a crystallizer unit with a final brine TDS of more than 30%. They reported an overall water recovery of 97–98% of brackish water. Similarly, Loganathan et al. [14] reported the treatment of basal water with a hybrid EDR-RO process followed by a low-temperature crystallizer for near-zero liquid discharge. The combined EDR-RO-crystallizer ZLD system achieved a TDS of 239,000 mg/L. A membrane distillation – crystallization process offers an alternative hybrid approach for the ZLD treatment process. A ZLD system consisting of freeze desalination (FD) and membrane distillation-crystallization (MD-C) processes was mathematically examined by Lu et al. [15]. The effects of various parameters including MD feed and FD recovery ratio on system energy consumption were explored. They concluded that a high MD feed temperature and concentration, a low distillate temperature, and a large FD recovery ratio are preferred to reduce overall energy consumption. Edwie et al. [18] studied a membrane distillation –

crystallization system for concurrent productions of pure water and salt crystals from saturated brine solutions. They found that increasing feed temperature from 40 to 70 °C improves membrane flux but it rapidly declines with time at higher feed temperatures (60 and 70 °C) due to membrane scaling facilitated by salt oversaturation at the membrane boundary layer. Chen et al. [19] optimized operating parameters of a membrane distillation – crystallization process for zero liquid discharge treatment. They found that the feed and permeate flow rates are the primary factors controlling performance, whereas temperatures either on the feed or permeate sides are not the main factors. Schwantes et al. [20] performed a techno-economic comparison between a membrane distillation and an MVC system employed for the ZLD treatment of highly saline wastewaters. Their results showed that an MD-ZLD system could be up to 40% more efficient compared to its MVC-ZLD counterpart. However, membrane fouling at high brine concentrations is a major limitation of an MD-ZLD system on a large scale.

More recently, Boo et al. [21] demonstrated ZLD of high salinity brines using temperature swing solvent extraction technique. A low-polarity solvent (e.g., Diisopropylamine) with temperature-dependent water solubility was utilized to extract water from a saline feed. The salt precipitates were sieved off and water was separated from the solvent by applying a low-grade heat. However, the specific energy consumption of the new process was estimated to be high and about 172 kWh_{th}/m³ of the treated feedwater. Menon et al. [22] demonstrated a passive and non-contact approach to enhance solar evaporation with ZLD using a photo-thermal umbrella for localized heating at the water's surface. Due to the transparency of water at visible and near-infrared wavelengths, a depth of about 100 m is required for the complete absorption of solar radiation in conventional brine evaporation ponds. They utilized a selective solar absorber and a black body emitter to convert sunlight into mid-infrared radiation where radiation is absorbed within a 100- μ m layer (i.e., heat is localized at the surface). At a solar intensity of 1000 W/m², an increase in evaporation rate from 0.22 kg/m²-h with bulk heating to 0.49 kg/m²-h with localized heating was observed. In an alternative strategy, Finnerty et al. [23] developed a synthetic leaf made of graphene oxide for solar desalination with ZLD. Under 825 W/m² of solar intensity with water with zero salinity, they observed a steam generation rate of 2 L/m²-h with a light-to-vapor energy conversion ratio of 78%. The evaporation rate was almost inversely proportional to water salinity. Specifically, the evaporation rate decreased from 2 L/m²-h for freshwater to 0.71 L/m²-h for water with an initial salinity of 7.0% NaCl. However, an increase in salinity led to a severe accumulation of salt crystals on the leaf surface, thereby decreasing the rates of water transport and evaporation. Additionally, both aforementioned solar ZLD desalination approaches suffer from a low evaporation rate per unit area for industrial-scale ZLD applications.

The above literature review reveals that current ZLD systems primarily rely on a high-grade electrically-driven MVC approach to realize the brine crystallization required for the ZLD treatment process. While most existing industrial-scale ZLD systems aim to minimize the volume of concentrated brine entering the crystallizer unit, recent ZLD techniques suffer from either a high energy consumption, a low distillate generation intensity per land area utilized, or reliability (e.g., a discontinuous ZLD operation with severe salt accumulation). Therefore, introduction of new ZLD concepts leveraging alternative mechanisms for brine crystallization is of paramount importance to further reduce energy consumption and improve the reliability of the ZLD desalination process. Here, an innovative desiccant-based ZLD distillation system is proposed to replace the electrically-driven MVC-based brine crystallizers with an energy-efficient thermally-driven vapor compression concept for industrial-scale ZLD desalination plants. The low water vapor pressure environment required for the ZLD operation is established by the strong hygroscopic properties of the aqueous lithium bromide (LiBr) salt. In the following sections, first, the proposed desiccant-based ZLD concept is discussed. A detailed thermodynamic model of the system is then developed. Finally, the energy performance

and size of the desiccant-based ZLD desalination system at different thermodynamic conditions and recovery ratios are examined.

2. Concept

This research addresses the shortcomings inherent to current ZLD techniques by an innovative desiccant-based concept in which a multiple-effect distillation (MED) unit is uniquely embedded at the heart of an absorption-desorption system. Contrary to current energy-intensive ZLD approaches, the proposed technology employs an absorption-based thermally-driven vapor compressor concept to create a low vapor pressure environment required for the ZLD treatment. Here, the ZLD operation is realized by the absorption process in which a strong hygroscopic Lithium Bromide (LiBr) solution captures a large volume of water vapor from the brine slurry discharged from the final MED effect. The low water vapor pressure of the crystallizer unit at which both evaporation and absorption processes occur is determined by the equilibrium water vapor pressure of the LiBr solution. The desiccant solution is then pumped to a high-pressure desorber condition for subsequent desorption and condensation processes. This eliminates the need for energy-intensive electrically-driven mechanical vapor compressors currently employed in advanced brine crystallizers. Additionally, the equilibrium temperature of the LiBr solution is almost 20–30 °C higher than the equilibrium temperature of the brine slurry being vaporized for typical operating pressures. Despite the accompanying boiling point elevation, this temperature lift partially compensates the temperature drop between MED effects, thereby further improving the thermal desalination efficiency of the system.

Fig. 1 illustrates a detailed model of the proposed multiple-effect desiccant-based ZLD technology. The system consists of three main units: (i) a forced-circulation (FC) ZLD unit, (ii) a forward feed MED unit, and (iii) an aqueous LiBr desorption unit. The ZLD unit is comprised of the absorber, FC heat exchanger, condenser, and brine crystallizer modules. The thermal vapor compression process starts in the absorber module of the ZLD unit where the concentrated brine slurry leaving the last MED effect is vaporized and exothermically absorbed by the LiBr solution (cf. Fig. 1). Once the water vapor is absorbed, the weak LiBr solution is pumped from the ZLD unit to the desorption unit (DU). The water vapor is then endothermically desorbed and subsequently condensed and withdrawn from the system. The thermal energy required for the desorption process is supplied by an external heat source such as a hot motive steam line. The strong LiBr solution leaving the DU flows back to the absorber of the ZLD unit to complete the LiBr-water mixture loop.

Latent heat released in the condenser module of the desorber unit and absorption heat generated in the ZLD unit is collected by a closed thermal water loop to drive the first MED effect. Latent heat associated with the condensing distillate vapor of each MED effect is then successively utilized to drive subsequent MED effects. The vapor produced in the last MED effect is condensed in the forced-circulation brine heat exchanger. In the ZLD unit, the brine slurry is circulated between the crystallizer maintained at a low vapor pressure and the FC heat exchanger operating at a high brine pressure. The low-pressure environment of the crystallizer module is established by the strong LiBr solution. The high operating pressure of the brine heat exchanger minimizes scaling and clogging issues and allows the superheating of the hypersaline brine slurry. Here, the brine is concentrated beyond the solubility limit of contaminants resulting in the formation of salt crystals. Vaporized water is also absorbed into the LiBr solution to enable the ZLD treatment process.

3. Thermodynamic modeling

A comprehensive thermodynamic model is developed using Engineering Equation Solver (EES) to evaluate the energy consumption of the proposed ZLD technology. EES is a powerful simultaneous equation

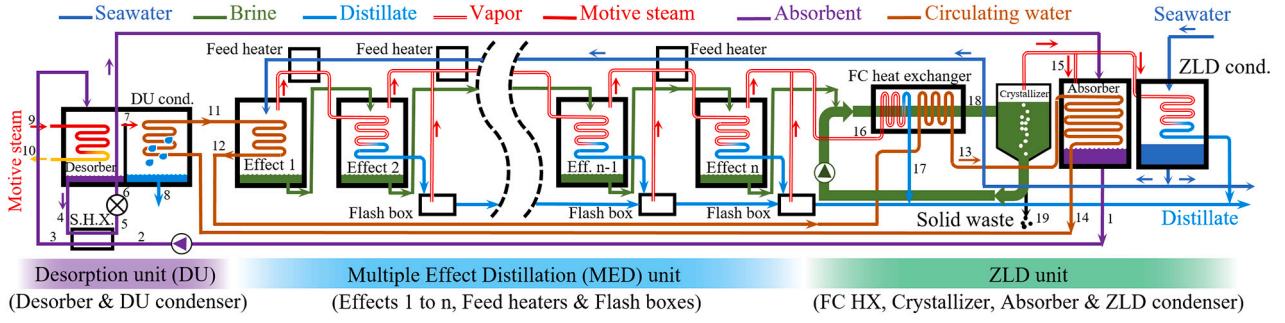


Fig. 1. A schematic diagram of the proposed sorption-based ZLD distillation system.

solver that includes a database of the necessary thermophysical properties of all working fluids employed in the system. The thermodynamic model includes the entire system shown in Fig. 1. The model developed by Mistry et al. [24] is used to formulate the MED sub-system. Seawater properties are evaluated as a function of temperature and salinity.

The following assumptions are made to perform the thermodynamic modeling of the system:

1. All involved processes are assumed to be steady-state.
2. Distilled water generated from the system is pure (i.e., the salinity of the distillate is 0 g/kg).
3. Seawater is incompressible and thermohydraulic properties are only functions of temperature and salinity.
4. Energy and pressure losses are negligible.
5. The solution leaving the absorber and desorber modules is at the vapor-liquid equilibrium state.

The modeling of each component is described in detail below.

3.1. Modeling of the ZLD unit

The operation of the ZLD unit is central to the proposed desalination concept. Fig. 2 shows a schematic of the ZLD unit. The brine from the last MED effect (B_n) is pumped at high pressures to the FC heat exchanger to get super-heated beyond the saturation temperature of the brine crystallizer. The FC brine heat exchanger is heated by the condensing distillate vapor of the last MED effect and the closed water loop leaving the first MED effect. In the brine crystallizer, the brine becomes super-saturated by the LiBr solution absorbing the water vapor. Here, the excess solute results in the formation of salt crystals that are continuously precipitated and removed from the brine slurry. The sub-atmospheric pressure of the brine crystallizer at which both evaporation and absorption processes occur is determined by the equilibrium water vapor pressure of the LiBr solution. The condensing distilled water in the FC brine heat exchanger (D_c^{FCHX}) is the sum of the distillate vapor generated in the last MED effect (D_n) and the flashed distillate vapor from the last flash box (D_{fb_n}).

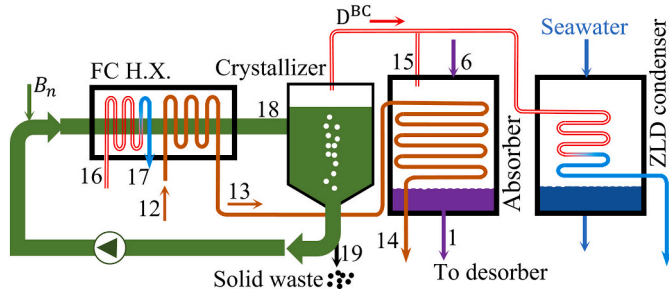


Fig. 2. A schematic of the ZLD unit consisting of the FC heat exchanger, brine crystallizer, absorber, and condenser modules.

$$D_c^{FCHX} = D_n + D_{fb_n} \quad (1)$$

The net feed brine entering the crystallizer (F^{BC}) is equal to the brine leaving the last MED effect (B_n). Therefore, the total mass and salt balance equations for the brine crystallizer can be expressed as:

$$F^{BC} = B_n = B^{BC} + D^{BC} \quad (2)$$

$$F^{BC} X_F^{BC} = B^{BC} X_B^{BC} \quad (3)$$

where F^{BC} is the feed stream of the brine crystallizer, B^{BC} is the solid crystal salts rejected from the system, D^{BC} is the distillate vapor generated in the brine crystallizer, X_F^{BC} is the salinity of the feed entering, and X_B^{BC} is the salt concentration for a complete distilled water removal process. At full ZLD operation, the recovery ratio (RR) defined as the desalinated water volume to the feed seawater volume is 95.6% (i.e., 100% ZLD operation).

The combined energy balance equation for the FC heat exchanger and the brine crystallizer modules can be written as:

$$D_c^{FCHX} \Delta h_{D_c}^{FCHX} + \dot{m}_{loop} C_{p,water} (T_{12} - T_{13}) = D^{BC} h_D^{BC} + B^{BC} h_B^{BC} - F^{BC} h_F^{BC} \quad (4)$$

where $\Delta h_{D_c}^{FCHX}$ is enthalpy changes of the condensing distillate vapor, h_D^{BC} is the enthalpy of the distillate vapor generated in the crystallizer, h_B^{BC} is the enthalpy of the salt crystals leaving the brine crystallizer, and h_F^{BC} is the enthalpy of the feed brine entering the crystallizer.

The tube surface area of the FC heat exchanger (A^{FCHX}) can be also estimated as follows:

$$D_c^{FCHX} \Delta h_{D_c}^{FCHX} + \dot{m}_{loop} C_{p,water} (T_{12} - T_{13}) = U^{FCHX} A^{FCHX} (T_{tube}^{FCHX} - T_{shell}^{FCHX}) \quad (5)$$

where T_{tube}^{FCHX} is the average tube-side temperature of the FC heat exchanger, T_{shell}^{FCHX} is the average shell-side temperature of the FC heat exchanger, and U^{FCHX} is the overall heat transfer coefficient.

The absorber module provides the low partial water vapor pressure environment required for the ZLD operation. Part of the distillate vapor generated in the brine crystallizer is absorbed by the strong LiBr solution and the remaining distillate vapor is condensed in the ZLD condenser module (cf. Fig. 2). The heat of the exothermic absorption process is collected by the closed thermal water loop. More importantly, the amount of water vapor absorbed by the LiBr solution (ϕD^{BC}) is defined by the heat required for the first MED effect and the ZLD unit.

The mass balance equations between streams of the absorber module can be written as:

$$\dot{m}_{15} = \phi D^{BC} \quad (6)$$

$$\dot{m}_1 = \dot{m}_{15} + \dot{m}_6 \quad (7)$$

$$\dot{m}_1 x_1 = \dot{m}_6 x_6 \quad (8)$$

where \dot{m}_{15} is the mass flow rate of the distilled vapor absorbed by the LiBr solution, and ϕ is the mass fraction of the distillate vapor absorbed. Here, \dot{m}_1 is the mass flow rate of the LiBr solution leaving the absorber

slightly below the saturation pressure, the distillate vapor generated in each effect is a combination of flash evaporation (D_f) and boiling (D_b). The portion of the feed brine before the boiling process is called the brine within each effect (B_{we}). Therefore, a portion of the brine within each effect is vaporized forming the distillate boiling (D_b) and the concentrated brine (B). The mass and salt balance equations between the incoming and outgoing streams can be written as:

$$F = B + D \quad (22)$$

$$D = D_f + D_b \quad (23)$$

$$F = B_{we} + D_f \quad (24)$$

$$FX_F = BX_B \quad (25)$$

$$FX_F = B_{we}X_{B_{we}} \quad (26)$$

where F , B , D , B_{we} , D_f and D_b are mass flow rates of the brine feed entering the effect, the brine leaving the effect, the distillate vapor generated in the effect, the brine within each effect, the distillate vapor generated by flash evaporation, and the distillate vapor generated by boiling, respectively. Also, X_F , X_B and $X_{B_{we}}$ are salinity of the feed, the brine leaving the effect, and the brine within each effect, respectively.

The energy balance equations between streams entering and leaving each effect can be also expressed as:

$$D_c \Delta h_{D_c} + F h_F = D h_D + B h_B \quad (27)$$

$$F h_F = B_{we} h_{B_{we}} + D_f h_{D_f} \quad (28)$$

where D_c is the mass flow rate of the condensing distillate entering the effect, Δh_{D_c} is enthalpy changes of the condensing distillate, h_D is the enthalpy of the distillate vapor generated in the effect, h_B is the enthalpy of the brine leaving the effect, h_F is the enthalpy of the feed entering the effect, $h_{B_{we}}$ is the enthalpy of the brine within each effect, and h_{D_f} is the enthalpy of the distillate generated due to flashing. It should be mentioned that there is no flash evaporation associated with the first effect ($D_{f, 1st\ effect} = 0$) since the feed seawater brine entering the first effect is at a subcooled condition. Additionally, the heat required for the evaporation of the feed brine in the first effect is supplied by the closed water circulation loop. Therefore, the energy balance for the first effect can be modified as:

$$\dot{m}_{loop} C_{p,water} (T_{11} - T_{12}) = D_1 h_{D_1} + B_1 h_{B_1} - F_1 h_{F_1} \quad (29)$$

where \dot{m}_{loop} is the mass flow rate of the water circulation loop, $C_{p,water}$ is the specific heat of water, T_{11} is the temperature of the water entering the first effect, and T_{12} is the temperature of the water leaving the first effect.

The required tube surface area (A_e) of each effect for complete in-tube condensation can be calculated considering the temperature difference driving the condensation process between the tube ($T_{D_{sat}^{prev}}$) and shell (T_e) sides as follows:

$$D_c \Delta h_{D_c} = U_e A_e (T_{D_{sat}^{prev}} - T_e) \quad (30)$$

where $T_{D_{sat}^{prev}}$ is the saturation temperature of the distillate from the previous effect, T_e is the temperature of the effect, and U_e is the effect overall heat transfer coefficient.

In the flash box (cf. Fig. 4), the condensed distillate from the effect (D_c) and condensed distillate from the previous effects (D_{bd}^{in}) are mixed. Here, the mixed condensed distillate is depressurized to its current effect pressure (p_e) in which a part of the incoming distillate stream is then flash vaporized (D_{fb}). As shown in Fig. 4, the flashed distillate vapor leaving the flash box and the distillate vapor generated in the current effect are mixed in the feed heater before being condensed in the next effect. The remaining condensed distillate (D_{bd}) is also blown out to the

next flash box. The mass and energy balance equations for the flash box can be expressed as:

$$D_c + D_{bd}^{in} = D_{fb} + D_{bd} \quad (31)$$

$$D_c h_{D_c} + D_{bd}^{in} h_{bd}^{in} = D_{fb} h_{D_{fb}} + D_{bd} h_{D_{bd}} \quad (32)$$

where h_{D_c} , h_{bd}^{in} , $h_{D_{fb}}$ and $h_{D_{bd}}$ are enthalpies of the condensed distillate from the current effect, the distillate blown in from the previous flash box, the distillate flashed vaporized in the current flash box, and the distillate blown out from the current to the next flash box, respectively.

Feed heaters (cf. Fig. 4) preheat the seawater and thus reduce the thermal energy required in the first MED effect. Here, the heat, released by the partial condensation of the distillate vapor from the effect and the flashed distillate vapor from the flash box, is supplied to the feed seawater. A terminal temperature difference of 5 °C is considered to define the amount of heat transferred between the streams. The energy balance between the seawater and the distillate vapor in the feed heater can be written as:

$$(D + D_{fb}) (h_{D_c}^{in} - h_{D_c}^{out}) = \dot{m}_F (h_{m_F}^{out} - h_{m_F}^{in}) \quad (33)$$

$$(D + D_{fb}) (h_{D_c}^{in} - h_{D_c}^{out}) = U^{FH} A^{FH} (T_{m_F}^{in} - T_{m_F}^{out}) / \left(\ln \frac{T_{D_{c,sat}} - T_{m_F}^{out}}{T_{D_{c,sat}} - T_{m_F}^{in}} \right) \quad (34)$$

where $h_{D_c}^{in}$ is the enthalpy of the distillate vapor entering the feed heater, $h_{D_c}^{out}$ is the enthalpy of the distillate vapor leaving the feed heater, \dot{m}_F is the mass flow rate of the feed entering the feed heater, $h_{m_F}^{in}$ is the enthalpy of the feed seawater entering the feed heater, and $h_{m_F}^{out}$ is the enthalpy of the feed seawater leaving the feed heater.

Since the proposed system is a new desalination concept, the results obtained from the present model cannot be directly compared with experimental and simulation data available in the open literature. However, the thermodynamic modeling results of the MED unit can be compared against those of Mistry et al. [24]. In these simulations, input parameters provided to the MED model are similar to those of Mistry et al. [24]. Fig. 5 shows a comparison between performance ratios of the present model and those of Mistry et al. [24] at different recovery ratios. It is evident that the two models are in excellent agreement with a maximum deviation of less than 2%. The small differences between the results from the two models originate from variations in the estimation of brine properties at high salinity levels.

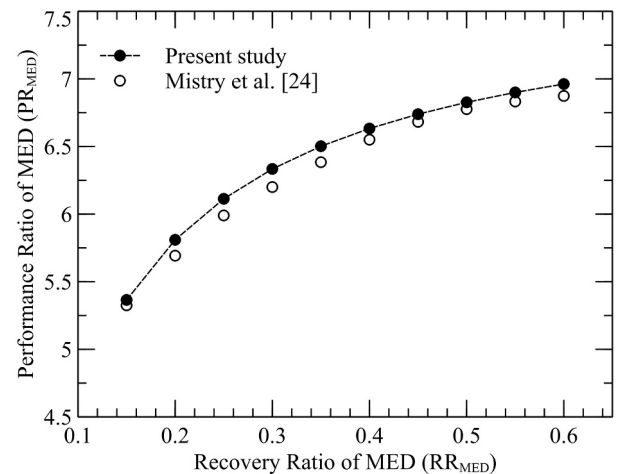


Fig. 5. A comparison between performance ratios of the present model with those of Mistry et al. [24].

4. Results and discussions

The thermodynamic model discussed above is employed to understand the energy performance and size of the proposed sorption-based ZLD desalination system at different thermodynamic conditions and MED recovery ratios. In this section, the proposed model is referred to as thermal vapor-compression or “thermal comp.” for short. Performance metrics of the proposed system are also studied at different numbers of MED effects to optimize system configuration. Additionally, the results are compared against a MED system coupled with an FC heat exchanger achieving the ZLD operation through thermal evaporation alone or “thermal evap.” for short. Furthermore, the energy performance of the proposed thermal evaporation based ZLD system is compared with an MVC-based ZLD system. Fig. 6 shows schematics of mechanical vapor compression, thermal evaporation, and proposed thermal vapor compression based ZLD system.

Fig. 7 shows the overall energy flow of the proposed sorption-based ZLD system with six MED effects at a MED recovery ratio of 80%. The MED recovery ratio represents the brine recovery ratio at the last stage of the MED unit before entering the ZLD unit. As shown, the system accepts 574.7 kW of thermal energy at 113 °C (i.e., T_9) to regenerate the LiBr solution in the desorber module, and rejects the same net energy through distillate in the MED, ZLD, and desorption units excluding the feedwater. It also shows the operating temperature range of each unit of the system. Table 2 summarizes the corresponding detailed operating conditions of the system shown in Fig. 7. The water vapor generated during the desorption process (i.e., point 7) condenses at a temperature of 89.9 °C in the DU condenser module. The 486.7 kW latent heat of the condensation process is harvested by the closed water circulation loop raising its temperature to 52.75 °C (i.e., T_{11}). The closed water loop delivers 861.1 kW thermal energy to the first MED effect generating distillate vapor at a temperature of 51.75 °C (i.e., T_{D1}). The latent heat of the condensing distillate vapor generated in each MED effect drives the next MED effect. The brine leaving the last MED effect at a temperature of 33 °C enters the FC heat exchanger and the brine crystallizer to get vaporized and thus achieve the ZLD operation. The latent heat required for the brine vaporization in the crystallizer module operating at a temperature of 29.25 °C (i.e., T_{18}) is supplied by the FC heat exchanger. The condensing distillate vapor of the last MED effect and the closed water circulation loop provides the heat required by the FC heat exchanger. Capturing the distillate vapor produced (i.e., point 15) in the ZLD unit, the strong LiBr solution leaving the desorber module (i.e., T_6) establishes the ZLD operating pressure of 4.067 kPa. The example shown here utilizes a total energy consumption of 66.65 kWh_{th}/m³ to achieve a complete ZLD operation.

Table 1
Constant input parameters considered for the thermodynamic model.

Parameter	Value
Brine crystallizer operating temperature, T^{BC}	29.25 °C
Boiling point elevation	1 °C
Seawater temperature at the inlet of the ZLD condenser, T_{sw}^{in}	23 °C
Seawater temperature at the outlet of the ZLD condenser, T_{sw}^{out}	27 °C
Temperature difference b/w MED effects, TTD_e	3.75 °C
Minimum terminal temperature difference b/w streams in feed heater, TTD_{FH}	5 °C
The mass flow rate of the feed seawater, \dot{m}_F	2.5 kg/s
The salinity of the feed, X_F	42 g/kg
Effectiveness of the solution heat exchanger, ϵ	0.8

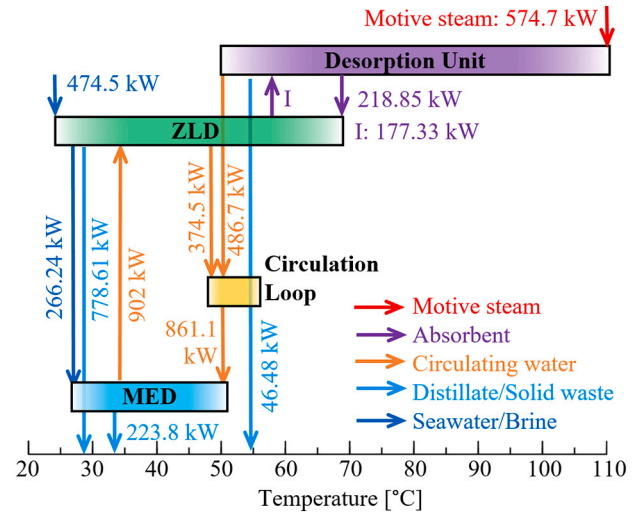


Fig. 7. Overall energy flow and respective unit temperature ranges of the proposed sorption-based ZLD system with six MED effects at a MED recovery ratio of 80%. The total mass flow rate of the distilled water produced is 2.395 kg/s.

Fig. 8 shows specific thermal energy required for the first MED effect of the proposed sorption-based ZLD system versus the MED recovery ratio (i.e., RR_{MED} or recovery ratio associated with the MED unit) at three MED effects. The specific thermal energy represents heat input per unit volume of water desalted. As shown, at a particular number of MED effects, the required thermal energy of the first MED effect increases as the quantity of high purity water produced increases (i.e., higher

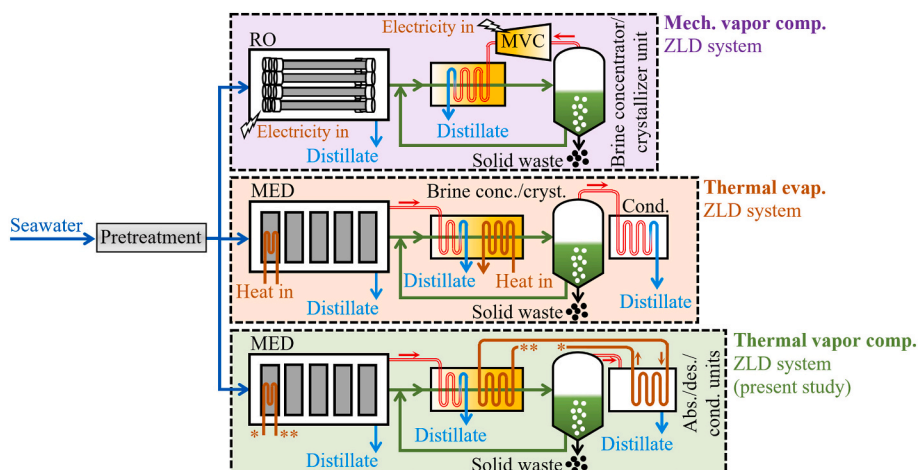


Fig. 6. Schematics of (a) a mechanical vapor compression, (b) a thermal evaporation, and (c) the proposed thermal vapor compression based ZLD system.

Table 2
Detailed operating conditions of the proposed sorption-based ZLD system with six MED effects at a MED recovery ratio of 80%.

Unit	Module	Point	T [°C]	P [kPa]	\dot{m} [kg/s]	X_{brine} or X_{LiBr}	
Desorption unit	Desorber (Q = 574.7 kW)	9 (motive steam)	113	–	0.2587	–	
		10 (motive steam)	113	–	0.2587	–	
		3 (LiBr)	91.15	16.15	1.291	0.5418	
		4 (LiBr)	112.50	16.15	1.091	0.6411	
	Condenser (Q = 486.7 kW)	7 (water vapor)	89.91	16.15	0.2	0 g/kg	
		8 (liquid water)	55.50	16.15	0.2	0 g/kg	
		11 (closed loop)	52.75	–	102.5	–	
	ZLD unit	Solution HX (Q = 84.53 kW)	2 (LiBr)	60.01	16.15	1.291	0.5418
			5 (LiBr)	70.50	16.15	1.091	0.6411
		Absorber (Q = 552.2 kW)	6 (LiBr)	70.50	4.067	1.091	0.6411
1 (LiBr)			60	4.067	1.291	0.5418	
Crystallizers		13 (circ. loop)	50.34	–	102.5	–	
		14 (circ. loop)	51.62	–	102.5	–	
	15 (water vapor)	29.25	4.067	0.2	0 g/kg		
	18 (brine slurry)	29.25	4.067	0.5	210 g/kg		
	19 (solid salt)	29.25	4.067	0.105	Pure salt		
FC HX (Q = 987.5 kW)	16 (water vapor)	33	5.035	0.3337	0 g/kg		
	17 (liquid water)	33	5.035	0.3337	0 g/kg		
	12 (circ. loop)	50.75	–	102.5	–		
MED unit	Effect 1 (Q = 861.1 kW)	Feed brine, F_1	46.75	13.47	2.5	42 g/kg	
		Distillate vapor, D_1	51.75	13.47	0.3411	0 g/kg	
	Effect 2 (Q = 775.3 kW)	Feed brine, F_2	51.75	13.47	2.159	48.64 g/kg	
		Distillate vapor, D_2	48	11.18	0.3382	0 g/kg	
	Effect 3 (Q = 776.7 kW)	Feed brine, F_3	48	11.18	1.821	57.67 g/kg	
		Distillate vapor, D_3	44.25	9.231	0.3354	0 g/kg	
	Effect 4 (Q = 778.2 kW)	Feed brine, F_4	44.25	9.231	1.485	70.69 g/kg	
		Distillate vapor, D_4	40.5	7.584	0.3326	0 g/kg	
	Effect 5 (Q = 779.7 kW)	Feed brine, F_5	40.5	7.584	1.153	91.09 g/kg	
		Distillate vapor, D_5	36.75	6.197	0.3298	0 g/kg	
	Effect 6 (Q = 771.2 kW)	Feed brine, F_6	36.75	6.197	0.8229	127.6 g/kg	
		Distillate vapor, D_6	33	5.035	0.3229	0 g/kg	

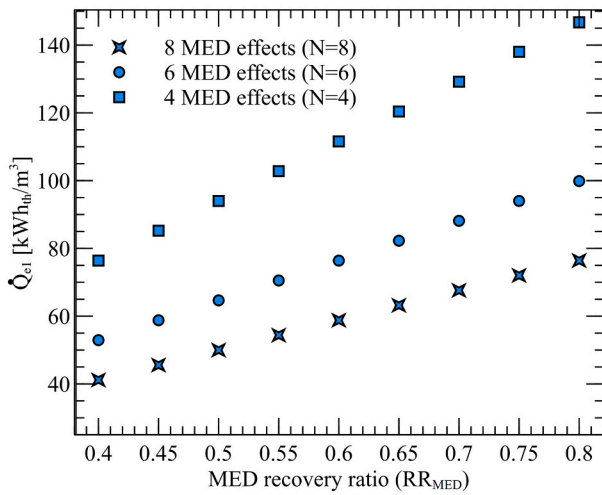


Fig. 8. Specific thermal energy of the first MED effect versus MED recovery ratio at three MED effects.

RR_{MED}). This is attributed to a larger amount of distillate vapor generated at higher recovery ratios of the MED unit, thus requiring additional input thermal energy for the evaporation process. Additionally, at a fixed recovery ratio, the thermal energy of the first MED effect per unit of distilled water produced decreases as the number of the MED effects increases. This is because the latent heat of the condensing distillate vapor is successively recovered through a larger number of the MED effects, thereby reducing the input thermal energy of the first MED effect.

The brine leaving the last MED effect enters the FC heat exchanger and brine crystallizer modules to be fully desalted. The specific thermal energy required for the ZLD treatment is partially supplied by the latent heat of the condensing distillate vapor leaving the last MED effect.

However, this heat is not sufficient to fully vaporize the brine slurry of the ZLD unit. Fig. 9 shows additional specific thermal energy required for a complete ZLD operation versus MED recovery ratio at three MED effects. As shown, the additional thermal energy of the ZLD unit per unit of the purified water generated decreases as the recovery ratio of the MED unit increases. This is because, at higher recovery ratios, the fraction of incoming feed seawater vaporized in the MED unit increases, thereby decreasing the required evaporation load of the ZLD unit. Furthermore, the additional specific thermal energy required for the ZLD treatment increases at higher numbers of MED effects. This is attributed to thermal energy exchanged per MED effect, which decreases as the number of the MED effects increases. This in turn reduces thermal energy supplied by the last MED effect to the FC heat exchanger, thereby

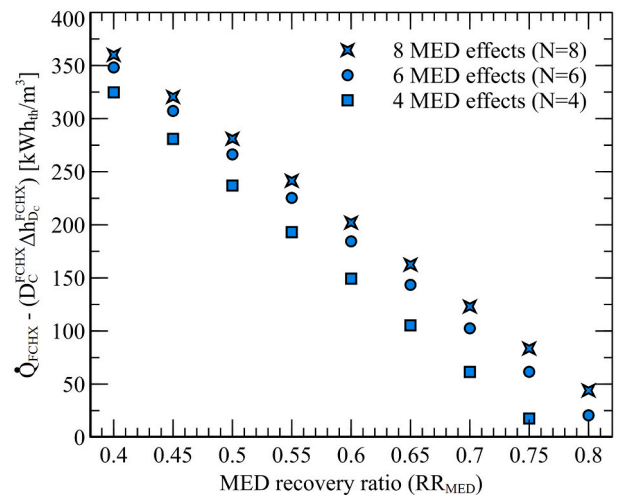


Fig. 9. Specific thermal energy of the ZLD unit versus MED recovery ratio at three MED effects.

increasing the external energy needed for the ZLD unit.

The water vapor produced in the ZLD crystallizer is partially absorbed by the strong hygroscopic LiBr solution of the absorber module. The absorbed water vapor is then thermally rejected in the desorption unit and subsequently condensed. The closed water circulation loop collects heat generated during the absorption process and latent heat released in the condenser module of the DU to supply additional thermal energy required for the ZLD treatment. Fig. 10 shows specific heat produced during the absorption process per unit of the desalinated water produced at different MED recovery ratios. As mentioned, the thermal evaporation load of the brine crystallizer decreases at higher recovery ratios of the MED unit. This in turn decreases the quantity of water vapor absorbed by the LiBr solution, thereby reducing the heat of the absorption process. It should be mentioned that the above trend is independent of the number of MED effects and only depends on the recovery ratios of the MED unit.

Fig. 11 shows the specific total thermal energy required by the proposed thermal compression based ZLD system per unit of the desalinated water produced at different MED recovery ratios. This thermal energy is supplied to the desorber module of the system. It is evident that the required specific thermal energy of the proposed thermal compression system decreases as the recovery ratio of the MED unit increases. This is because the additional energy required for the ZLD operation (cf. Fig. 9) significantly declines with the MED recovery ratio, thereby decreasing the total input thermal energy of the system at higher values of RR_{MED} .

Fig. 11 also shows that the specific total thermal energy of the proposed ZLD system is independent of the number of MED effects. The total thermal energy required by the system is the sum of the energy consumptions of the first MED effect and the FCHX. The energy consumption of the FCHX is supplied by the latent heat of the condensing distillate vapor leaving the last MED effect and the closed water circulation loop. At a fixed MED recovery ratio, the amount of distillate generated in each MED effect decreases as the number of MED effects increases. This subsequently reduces both the energy consumption of the first MED effect and the energy supplied to the FCHX by the condensing distillate vapor of the last MED effect. Therefore, the additional energy supplied to the FCHX to achieve the ZLD operation increases at a higher number of MED effects. However, the rise in the energy requirement of the FCHX module balances out the drop in the energy consumption of the first MED effect, thereby keeping the overall energy consumption independent of the number of MED effects.

Additionally, Fig. 11 shows specific thermal energy required by a multiple-effect thermal evaporation approach achieving the ZLD

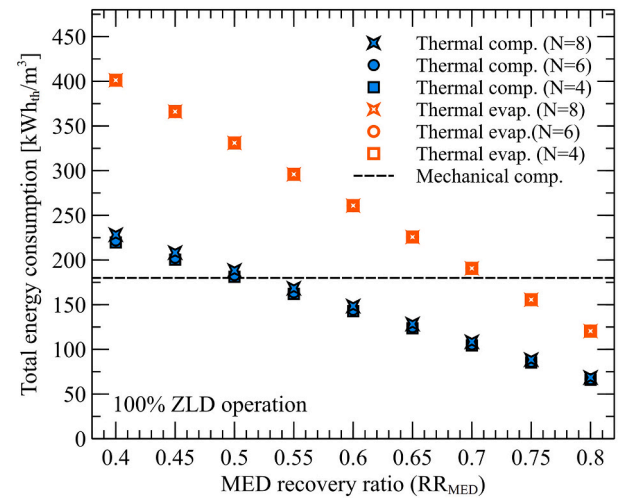


Fig. 11. Specific total energy required by the proposed ZLD system, thermal evaporation, and mechanical compression at different recovery ratios.

operation for comparison. In the thermal evaporation approach (cf. Fig. 6), the brine leaving the last MED effect is sent to a thermally driven FC heat exchanger module to be fully vaporized and then condensed by the cooling effect of the feed seawater (i.e., no absorber module is included). Furthermore, Fig. 11 shows the performance of an electrically-driven mechanical vapor compressor (i.e., mechanical compression) utilized in advanced ZLD brine crystallizers. A site-to-source energy conversion ratio of 3.06 with a combined electricity generation (i.e., in the power plant) and transmission efficiency of 32.6% is used to estimate equivalent thermal energy consumption. Consuming 52–66 kWh of electric energy per cubic meter of the distillate produced, state-of-the-art mechanical vapor compression based ZLD systems have an equivalent thermal energy usage of 160–200 kWh per cubic meter of the water distilled [3]. On the other hand, the proposed thermal compression based ZLD system directly utilizes thermal energy and thus excludes inefficiencies associated with the conversion of thermal to electric energy. As shown, the required specific thermal energy of the proposed thermal vapor-compression-based system is significantly lower than that of both thermal evaporation and mechanical vapor compression based ZLD approaches owing to the harvesting of the latent heats generated by the ZLD absorber and DU condenser modules. At a MED recovery ratio of 80%, the proposed desiccant-based ZLD concept demonstrates an energy consumption of 67 kWh of thermal energy per cubic meter of the distillate produced. This is a 63% reduction in the ZLD energy consumption compared with advanced MVC-based ZLD systems with an average equivalent thermal energy usage of 180 kWh_{th}/m³. Compared with thermal evaporation based ZLD systems with an energy usage of about 120 kWh_{th}/m³ at a MED recovery ratio of 80%, the specific energy consumption of the ZLD process is improved by 44%.

Fig. 12 shows the gained output ratio (GOR) of the proposed ZLD desalination system and a thermal evaporation based ZLD approach at different MED recovery ratios. The GOR representing the first law efficiency of a desalination plant is defined as the heat required to evaporate the desalted water to that of the system input. As shown, the GOR of the proposed ZLD system increases with the recovery ratio of the MED unit. This is attributed to the total thermal energy of the system (cf. Fig. 11), which decreases as the recovery ratio of the MED unit increases. Additionally, the GOR of the proposed ZLD system is significantly higher than that of the thermal evaporation based ZLD approach (e.g., 10 versus 5.6 at a MED recovery ratio of 80%) due to the difference between their input thermal energy levels (cf. Fig. 11). It can be also seen that GOR of both thermal compression and evaporation systems achieving the ZLD operation are insensitive to the number of MED effects.

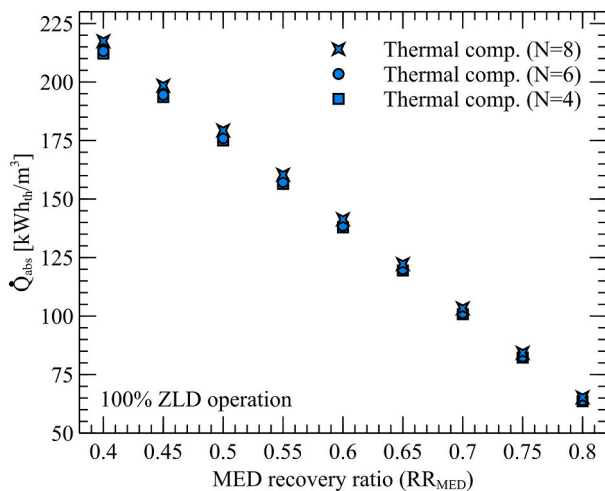


Fig. 10. Specific heat released during the absorption process versus MED recovery ratio at three MED effects.

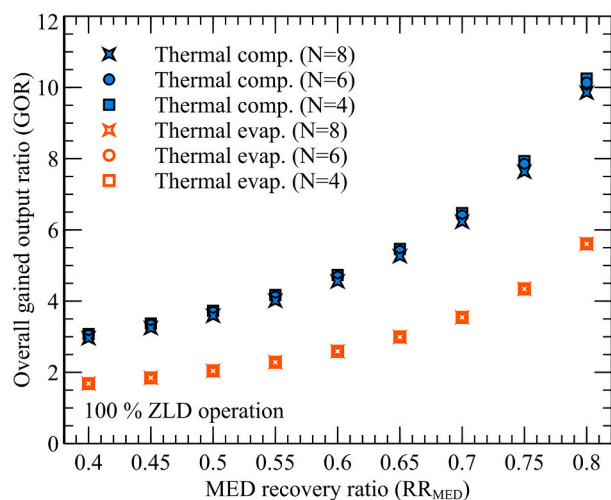


Fig. 12. Overall gained output ratio of the proposed ZLD system and thermal evaporation at different MED recovery ratios.

Fig. 13 shows the required overall heat transfer coefficient (i.e., UA) of the proposed ZLD system per unit of the distilled water produced at different MED recovery ratios. While the GOR represents the operating expense (OPEX) of a desalination plant, the specific overall UA indicates the capital expenditure (CAPEX) of the plant. As shown, for a fixed MED recovery ratio, the specific overall UA required by the proposed ZLD system or a thermal evaporation based ZLD system decreases with the number of the MED effects. This is mainly because of a fixed logarithmic mean temperature difference (LMTD) assumed across each MED effect (cf. Table 1), which increases the overall LMTD across the entire MED unit as the number of the MED effects increases. This in turn reduces the overall required UA per unit of product water. Additionally, the specific overall UA decreases at higher recovery ratios of the MED unit. This can be attributed to the total overall UA required by the ZLD and desorption units, which decreases as the recovery ratio of the MED unit increases. Furthermore, the specific overall UA of the proposed sorption-based ZLD system is higher than that of the thermal evaporation based ZLD system mainly due to the additional heat transfer area required by the absorber and desorber modules. In other words, the proposed sorption-based thermal compression ZLD system offers a lower OPEX but a higher CAPEX compared to a thermal-evaporation-based ZLD system.

5. Conclusions

In this study, a novel desiccant-based ZLD desalination concept was proposed to fully recover the liquid waste and salt crystals from a hypersaline brine solution. The new ZLD system relies on the strong hygroscopic properties of a liquid-desiccant solution to capture a large volume of water vapor from the brine slurry and pressurize it to a high-pressure desorber module. This replaces the energy-intensive electrically-driven mechanical vapor compressors currently utilized in state-of-the-art brine crystallizers with an energy-efficient thermally-driven vapor-compression-based brine crystallizer. The energy performance and size of the proposed ZLD system were comprehensively analyzed through detailed thermodynamic modeling at various thermohydraulic conditions.

The results indicated that the ZLD energy efficiency of the proposed desiccant-based system is higher than that of both thermal evaporation and mechanical vapor compression approaches due to the harvesting of the latent heats generated during absorption and condensation processes. In particular, the first law efficiency (i.e., GOR) of the proposed desiccant-based ZLD system is 10 compared with a GOR of 5.6 for a thermal evaporation process at a MED recovery ratio of 80%. Additionally, the energy consumption of the proposed ZLD system is 67 kWh

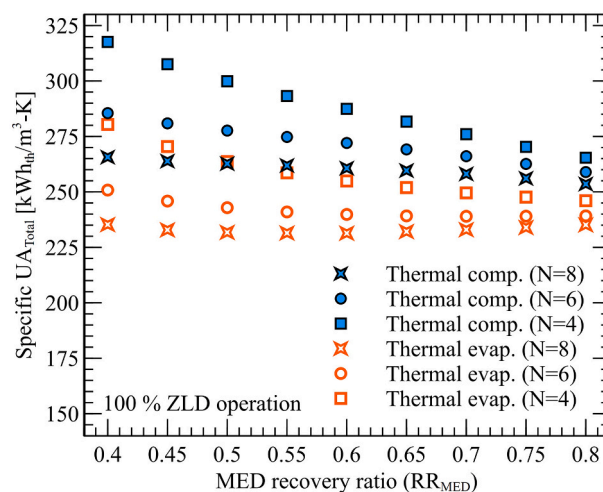


Fig. 13. Specific overall heat transfer coefficient of the proposed ZLD system and thermal evaporation at different MED recovery ratios.

of thermal energy per cubic meter of the distillate produced, reflecting 63% and 44% reductions in the ZLD energy consumption compared with advanced MVC and thermal evaporation based ZLD systems, respectively.

In summary, the present study confirms that the proposed multiple-effect desiccant-based ZLD desalination concept could offer new pathways for ZLD treatment of high salinity brines in a promising energy-efficient and economical manner. In the future, the technical viability of the desiccant-based ZLD system will be experimentally examined. Additionally, the performance of the proposed ZLD system with emerging ionic liquid desiccants that could minimize crystallization risks and corrosion issues typically associated with a LiBr solution will be studied.

CRedit authorship contribution statement

Sunil Pinnu: Investigation, Data curation, Visualization, Writing - Original draft preparation

Sajjad Bigham: Conceptualization, Supervision, Methodology, Visualization, Writing - Original draft preparation, Writing - Reviewing and Editing

Declaration of competing interest

The authors declare that they have no known competing financial interests or personal relationships that could have appeared to influence the work reported in this paper.

Acknowledgements

This study was sponsored by the US Department of Energy's Office of Energy Efficiency and Renewable Energy (EERE) under the Solar Desalination Prize of the Solar Energy Technologies Office (SETO).

References

- [1] M. Elimelech, W.A. Phillip, The future of seawater desalination: energy, technology, and the environment, *Science*. 333 (2011) 712–717, <https://doi.org/10.1126/science.1200488>.
- [2] R. Kaplan, D. Mamrosh, H.H. Salih, S.A. Dastgheib, Assessment of desalination technologies for treatment of a highly saline brine from a potential CO2 storage site, *Desalination*. 404 (2017) 87–101, <https://doi.org/10.1016/j.desal.2016.11.018>.
- [3] T. Tong, M. Elimelech, The global rise of zero liquid discharge for wastewater management: drivers, technologies, and future directions, *Environ. Sci. Technol.* 50 (2016) 6846–6855, <https://doi.org/10.1021/acs.est.6b01000>.

- [4] R.L. McGinnis, N.T. Hancock, M.S. Nowosielski-Slepowron, G.D. McGurgan, Pilot demonstration of the NH₃/CO₂ forward osmosis desalination process on high salinity brines, *Desalination*. 312 (2013) 67–74, <https://doi.org/10.1016/j.desal.2012.11.032>.
- [5] N. Afrasiabi, E. Shahbazali, RO brine treatment and disposal methods, *Desalin. Water Treat.* 35 (2011) 39–53, <https://doi.org/10.5004/dwt.2011.3128>.
- [6] A. Giwa, V. Dufour, F. Al Marzooqi, M. Al Kaabi, S.W. Hasan, Brine management methods: recent innovations and current status, *Desalination*. 407 (2017) 1–23, <https://doi.org/10.1016/j.desal.2016.12.008>.
- [7] M. Ahmed, W.H. Shayya, D. Hoey, A. Mahendran, R. Morris, J. Al-Handaly, Use of evaporation ponds for brine disposal in desalination plants, *Desalination*. 130 (2000) 155–168, [https://doi.org/10.1016/S0011-9164\(00\)00083-7](https://doi.org/10.1016/S0011-9164(00)00083-7).
- [8] D.L. Shaffer, L.H. Arias Chavez, M. Ben-Sasson, S. Romero-Vargas Castrillón, N. Y. Yip, M. Elimelech, Desalination and reuse of high-salinity shale gas produced water: drivers, technologies, and future directions, *Environ. Sci. Technol.* 47 (2013) 9569–9583, <https://doi.org/10.1021/es401966e>.
- [9] A. Pérez-González, A.M. Urtiaga, R. Ibáñez, I. Ortiz, State of the art and review on the treatment technologies of water reverse osmosis concentrates, *Water Res.* 46 (2012) 267–283, <https://doi.org/10.1016/j.watres.2011.10.046>.
- [10] A. Subramani, J.G. Jacangelo, Treatment technologies for reverse osmosis concentrate volume minimization: a review, *Sep. Purif. Technol.* 122 (2014) 472–489, <https://doi.org/10.1016/j.seppur.2013.12.004>.
- [11] X. Ji, E. Curcio, S. Al Obaidani, G. Di Profio, E. Fontananova, E. Drioli, Membrane distillation-crystallization of seawater reverse osmosis brines, *Sep. Purif. Technol.* 71 (2010) 76–82, <https://doi.org/10.1016/j.seppur.2009.11.004>.
- [12] H. Guo, H.M. Ali, A. Hassanzadeh, Simulation study of flat-sheet air gap membrane distillation modules coupled with an evaporative crystallizer for zero liquid discharge water desalination, *Appl. Therm. Eng.* 108 (2016) 486–501, <https://doi.org/10.1016/j.applthermaleng.2016.07.131>.
- [13] Y. Oren, E. Korngold, N. Daltrophe, R. Messalem, Y. Volkman, L. Aronov, M. Weismann, N. Bouriakov, P. Glueckstern, J. Gilron, Pilot studies on high recovery BWRO-EDR for near zero liquid discharge approach, *Desalination*. 261 (2010) 321–330, <https://doi.org/10.1016/j.desal.2010.06.010>.
- [14] K. Loganathan, P. Chelme-Ayala, M. Gamal El-Din, Treatment of basal water using a hybrid electro dialysis reversal-reverse osmosis system combined with a low-temperature crystallizer for near-zero liquid discharge, *Desalination*. 363 (2015) 92–98, <https://doi.org/10.1016/j.desal.2015.01.020>.
- [15] K.J. Lu, Z.L. Cheng, J. Chang, L. Luo, T.S. Chung, Design of zero liquid discharge desalination (ZLDD) systems consisting of freeze desalination, membrane distillation, and crystallization powered by green energies, *Desalination*. 458 (2019) 66–75, <https://doi.org/10.1016/j.desal.2019.02.001>.
- [16] D.G. Randall, J. Nathoo, A.E. Lewis, A case study for treating a reverse osmosis brine using eutectic freeze crystallization-approaching a zero waste process, *Desalination*. 266 (2011) 256–262, <https://doi.org/10.1016/j.desal.2010.08.034>.
- [17] S.O. Odu, A.G.J. Van Der Ham, S. Metz, S.R.A. Kersten, Design of a process for supercritical water desalination with zero liquid discharge, *Ind. Eng. Chem. Res.* 54 (2015) 5527–5535, <https://doi.org/10.1021/acs.iecr.5b00826>.
- [18] F. Edwie, T.S. Chung, Development of simultaneous membrane distillation-crystallization (SMDC) technology for treatment of saturated brine, *Chem. Eng. Sci.* 98 (2013) 160–172, <https://doi.org/10.1016/j.ces.2013.05.008>.
- [19] G. Chen, Y. Lu, W.B. Krantz, R. Wang, A.G. Fane, Optimization of operating conditions for a continuous membrane distillation crystallization process with zero salty water discharge, *J. Membr. Sci.* 450 (2014) 1–11, <https://doi.org/10.1016/j.memsci.2013.08.034>.
- [20] R. Schwantes, K. Chavan, D. Winter, C. Felsmann, J. Pfafferoth, Techno-economic comparison of membrane distillation and MVC in a zero liquid discharge application, *Desalination*. 428 (2018) 50–68, <https://doi.org/10.1016/j.desal.2017.11.026>.
- [21] C. Boo, I.H. Billinge, X. Chen, K.M. Shah, N.Y. Yip, Zero liquid discharge of ultrahigh-salinity brines with temperature swing solvent extraction, *Environ. Sci. Technol.* 54 (2020) 9124–9131, <https://doi.org/10.1021/acs.est.0c02555>.
- [22] A.K. Menon, I. Haechler, S. Kaur, S. Lubner, R.S. Prasher, Enhanced solar evaporation using a photo-thermal umbrella for wastewater management, *Nat. Sustain.* 3 (2020) 144–151, <https://doi.org/10.1038/s41893-019-0445-5>.
- [23] C. Finnerty, L. Zhang, D.L. Sedlak, K.L. Nelson, B. Mi, Synthetic graphene oxide leaf for solar desalination with zero liquid discharge, *Environ. Sci. Technol.* 51 (2017) 11701–11709, <https://doi.org/10.1021/acs.est.7b03040>.
- [24] K.H. Mistry, M.A. Antar, J.H. Lienhard V, An improved model for multiple effect distillation, *Desalin. Water Treat.* 51 (2013) 807–821, <https://doi.org/10.1080/19443994.2012.703383>.